

# Battery-operated mid-infrared diode laser frequency combs

Lukasz A. Sterczewski<sup>1,2,\*</sup>, Mathieu Fradet<sup>1</sup>, Clifford Frez<sup>1</sup>, Siamak Forouhar<sup>1</sup>,  
and Mahmood Bagheri<sup>1,†</sup>

<sup>1</sup>Jet Propulsion Laboratory, California Institute of Technology, Pasadena, CA 91109, USA

<sup>2</sup>Faculty of Electronics, Photonics and Microsystems, Wrocław University of Science and Technology, Wyb. Wyspińskiego 27, 50-370 Wrocław, Poland

Mid-wave infrared (MIR, 3–5  $\mu\text{m}$ ) optical frequency combs (OFC) are of critical importance for spectroscopy of fundamental molecular absorption features in space and terrestrial applications. Although in this band OFCs can be obtained via supercontinuum or difference frequency generation using optical pumping schemes, unprecedented source miniaturization and monolithic design are unique to electrically-pumped semiconductor laser structures. To date, high-brightness OFC generation in this region has been demonstrated in quantum- and interband cascade lasers (QCL/ICL), yet with sub-optimal spectral properties. Here, we show the first MIR quantum well diode laser (QWDL) OFC, whose excellent spectral uniformity, narrow optical linewidths, and milliwatt optical power are obtained at a fraction of a watt of power consumption. The continuously tunable source offers  $\sim 1$  THz of optical span centered at 3.04  $\mu\text{m}$ , and a repetition rate of 10 GHz. As a proof-of-principle, we show a directly-battery-operated MIR dual-comb source with almost 0.5 THz of optical coverage accessible in the electrical domain in microseconds. These results indicate the high suitability of QWDL OFCs for future chip-based real-time sensing systems in the mid-infrared.

## Introduction

Access to the mid-infrared (MIR) spectral region (3–5  $\mu\text{m}$ ) plays a vital role for molecular spectroscopy due to the presence of strong ro-vibrational transitions of many environmentally-important species in this band. High sensitivity and selectivity makes trace gas monitoring, breath analysis, and industrial quality control particularly attractive in the MIR. While spectrally-broadband emission in this region can be obtained using thermal incoherent sources such as globars<sup>1</sup>, revolutionary new coherent light emitters offer unmatched optical power and the discrete structure of an optical frequency comb (OFC)<sup>2</sup>. The latter feature enables performing precise, broadband and high-resolution measurements in the moving-parts-free configuration of a dual-comb spectrometer (DCS)<sup>3</sup>, which naturally links the optical and radio-frequency domain with equivalent spectral sweep times reaching microseconds.

Despite many technological challenges, the importance of the MIR region has driven extensive research on OFC generation. In principle, many novel platforms offer octave-wide coverages, yet they still require bulky external pump lasers. This is in stark contrast to emerging battery-operated fully-integrated systems at telecom wavelengths<sup>4</sup>. An alternative way to generate MIR OFCs is exploiting intracavity optical nonlinearities in monolithic semiconductor lasers, which combine direct MIR OFC emission with high-power per comb line, wavelength tunability, and extremely small footprint<sup>5</sup>. Moreover, the bifunctionality of semiconductor lasers<sup>6,7,8</sup> promises fully-integrated dual-comb sources and detectors defined photolithographically on the same chip.

To date, MIR OFC generation in semiconductor lasers has been demonstrated in quantum cascade lasers (QCL)<sup>9</sup>, type-II<sup>10,11,7</sup>, and type-I<sup>12</sup> interband *cascade* lasers (ICLs). Semiconductor laser combs offer terahertz-wide optical coverages and gigahertz repetition rates resulting in micro-to-milliwatt optical power per comb line. Unfortunately, the performance of the most widespread QCL comb platform drastically degrades at shorter wavelengths ( $< 5$   $\mu\text{m}$ ), which relates to problematic dispersion compensation<sup>13</sup> and excitation of harmonic states with high modal sparsity<sup>14</sup>. Furthermore, the multi-watt power consumption hinders thermal and power management for QCL-based sensors. The recently demonstrated type-II ICL combs are an interesting alternative to QCLs with battery-compatible sub-watt power consumption and suitability for free-running DCS, yet their spectral properties in low-noise comb regimes remain plagued by the same issues as in short-wavelength QCLs; namely high modal sparsity due to harmonic/quasi-harmonic operation<sup>15</sup>. Mode grouping phenomena can be also added to this list.<sup>7,11</sup> Type-I ICL combs, in turn, have shown stable mode-locked comb generation only in external optical feedback configurations<sup>16</sup> with reduced optical bandwidths and a loss of the monolithic design. Therefore, there is an exceedingly important niche for stable monolithic comb lasers to cover the organic C-H stretch band around 3  $\mu\text{m}$ , associated with the existence of life-related molecules.

Here, we address this demand and present a monolithic MIR OFC platform exploiting a GaSb-based type-I quantum well diode laser (QWDL) medium, whose comb operation was previously restricted only to the

\*lukasz.sterczewski@pwr.edu.pl

†mahmood.bagheri@jpl.nasa.gov

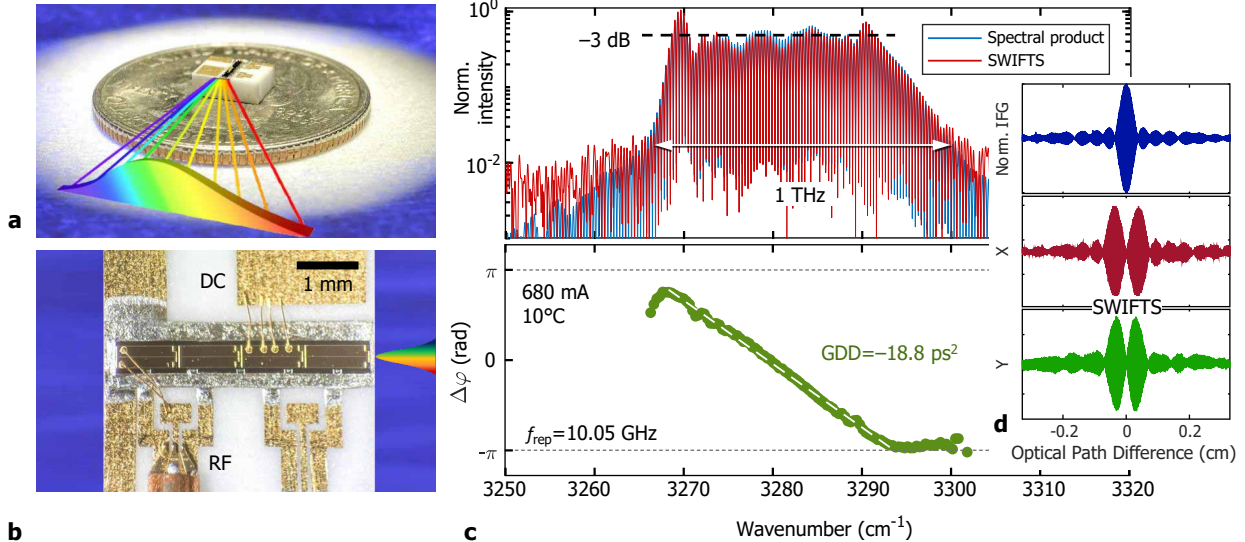


**Figure 1 – Mid-infrared quantum well diode laser frequency combs.** **a:** Picture of a device mounted onto a BeO submount. **b:** Micrograph of the same device showing the radio-frequency (RF) signal extraction scheme with a microwave probe, and a DC bias pad. **c:** Intensity and phase spectra obtained in the SWIFTS analysis at 680 mA of injection current. **d:** Normal (DC) and quadrature (X/Y) SWIFTS IFGs proving frequency-modulated emission.

near-infrared<sup>17</sup>. Our devices emitting around 3  $\mu\text{m}$  offer excellent comb coherence over a 1 THz optical bandwidth with almost flat single-lobed spectra. Sub-megahertz optical linewidths exhibited by the devices are fully compatible with free-running DCS. The diodes can be directly powered from AA batteries, which was used here to demonstrate a working, battery-operated MIR dual-comb source for mode-resolved spectroscopy. This platform also addresses the critical demand for spectrally-uniform stable comb sources without gaps in the emitted spectrum, mode clustering issues<sup>18</sup> or operation in harmonic<sup>19</sup>/quasi-harmonic states<sup>10,20</sup>, which is a prerequisite for widespread adoption of chip-scale DCS beyond research laboratories.

## Results and Discussion

**Comb properties** To assess the frequency comb characteristics of MIR QWDLs, we mounted a 4 mm long single-section device (see Methods for structure details) onto a radio-frequency (RF) compatible submount (Fig. 1a–b), and performed a linear interferometric measurement known as shifted wave interference Fourier transform spectroscopy (SWIFTS)<sup>21</sup>. This well-established technique allows for characterization of the coherence and relative phase between all comb lines in the spectrum (see Methods) without resorting to nonlinear interferometric or intensity autocorrelation, which remain experimentally challenging at longer wavelengths. Instead, SWIFTS simultaneously records a normal (DC) and microwave ( $f_{\text{rep}}$ ) interferograms (IFGs) from a fast linear photodetector. The results of the

analysis are plotted in Fig. 1c. First, the device shows a remarkably uniform spectrum for a semiconductor OFC: the envelope has a single lobe with  $\sim 3$  dB intensity variations relative to the mean in the dominant part. This spectral pattern is observed at all currents exceeding the multimode operation threshold ( $\sim 2.5 \times$  lasing threshold  $J_{\text{th}}$ ) and is a distinct feature of this OFC platform. 15 milliwatts of optical power per facet are spread over 100 lines constituting the 20 dB optical bandwidth of 1 THz. Pronounced modal intensities around the spectral edges suggest strong frequency modulation (FM), which is expected for single-section semiconductor laser devices that obtain comb emission through an interplay of spatial hole burning and four-wave mixing<sup>22,23</sup>. The agreement between the spectral product (square root of the intensity spectrum product with an  $f_{\text{rep}}$ -shifted replica), and the SWIFTS intensity spectrum proves that all lines contribute to comb emission. The intermodal phases spanned over almost a full range from  $-\pi$  to  $\pi$  indicate maximally chirped emission<sup>22,23</sup> with an equivalent group delay dispersion of the electric field in the linear part of  $-18.8$  ps<sup>2</sup>. However, the shape deviates from a perfectly linearly chirped source, which is due to higher order dispersion of the generated waveform’s electric field. It manifests itself as oscillations and intermodal phase flattening close to the spectral edges. A minimum in the SWIFTS quadratures (X/Y) where the normal (DC) IFG has a maximum is also a signature of strong FM, like previously observed in near-infrared QWDL combs<sup>17</sup>.

**Suitability for free-running DCS** Whereas SWIFTS gives access to relative phase coherence, it

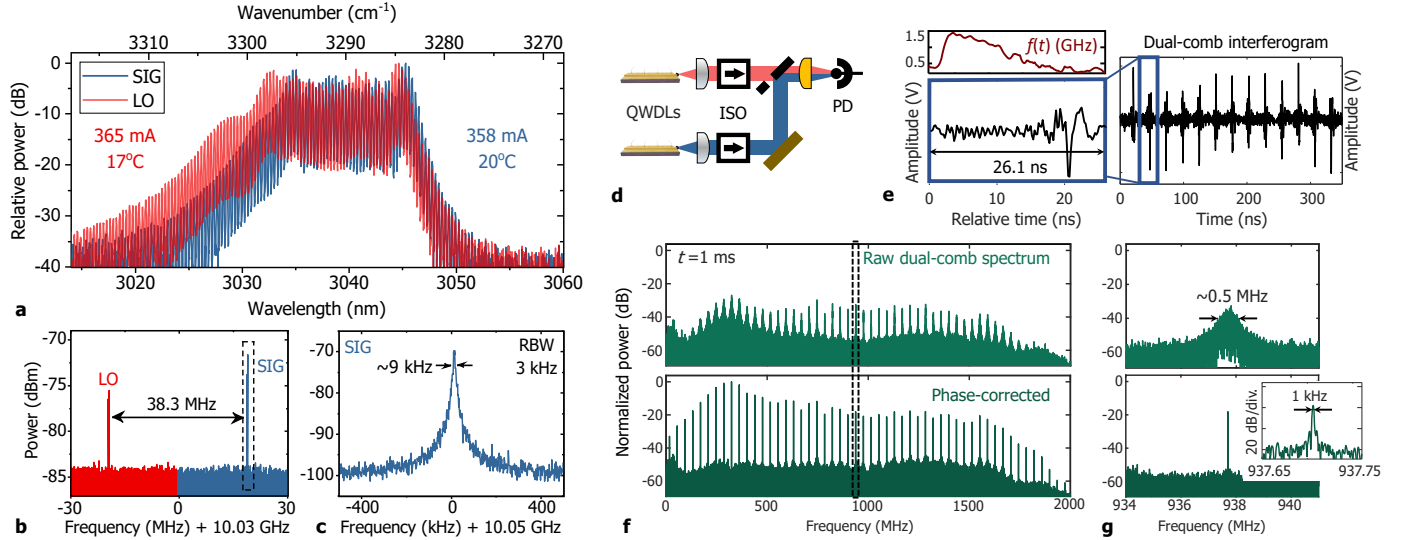


**Figure 2 – Dual-comb beating of two free-running 3  $\mu\text{m}$  wavelength comb laser diodes.** **a:** Optical spectra measured with a fiber-coupled spectrum analyzer. **b:** Optically detected intermode beat notes. **c:** Zoom on the signal (SIG) comb's intermode beatnote. **d:** Experimental setup. Two QWDLs were optically-isolated (ISO) prior to combining on a photodetector (PD). **e:** Dual-comb IFG measured from the photodetector's RF port along with a zoom on a single period. The retrieved instantaneous frequency  $f(t)$  of the IFG shows strong linear chirp. **f:** Raw (top) and digitally-corrected (bottom) dual-comb spectrum. The optical coverage is 520 GHz (limited by the oscilloscope). **g:** Zoom on the center beat note before and after correction.

does not provide information about absolute comb stability i.e. optical linewidth. To prove the excellent suitability of the MIR QWDL OFCs for demanding heterodyne measurements, we optically beat a pair of length-mismatched sources (several  $\mu\text{m}$ ) with a repetition rate mismatch of  $\Delta f_{\text{rep}} = 38.3$  MHz. The light from the devices was spatially and spectrally overlapped onto a fast 3  $\mu\text{m}$  photodetector, and next the resulting DCS beating signal was recorded with an oscilloscope (see Methods). Along with the lower-frequency DCS beating signal, we measured its high-frequency portion (near  $f_{\text{rep}}$ ) using an RF spectrum analyzer to quantify the timing stability.

At injection currents of approximately  $\sim 360$  mA and bias voltages of  $\sim 1.3$  V, the devices developed 6 mW of optical power with  $\sim 0.5$  THz 10 dB bandwidths (Fig. 2a) and kilohertz-wide intermode beat notes (Fig. 2b,c). Such conditions were chosen to promote operation in the low group velocity dispersion (GVD) region (discussed later in the text) with narrow optical linewidths observable as sharp and intensive dual-comb lines. While at higher injection currents the devices should still possess the equidistance properties of an OFC as evident from the SWIFTS analysis, more phase noise was observed in the DCS signal seen as multi-megahertz-wide DCS beatnotes. To ensure the unperturbed operation of the combs, we used optical isolators for suppressing unwanted delayed optical feedback (Fig. 2d).

Because the DCS technique gives access to the cross-correlation of the combs' electric fields, some of the temporal characteristics can be retrieved directly from the beating signal. To achieve that, we analyzed the time-domain

electrical IFG shown in Fig. 2e, which has a clear periodic structure with a non-zero offset frequency seen as an evolution of the waveform from frame to frame lasting 26.1 ns. Unexpectedly, it resembles a train of pulses followed by a noise-like oscillatory response. In fact, it is a highly chirped waveform that starts at a high frequency ( $\sim 1.5$  GHz, top panel), and gradually progresses toward lower frequencies. Due to the higher beat note amplitudes around 300–400 MHz, the IFG's amplitude increases as it approaches the lower frequency region, which potentially explains its pulsed-like shape. Nevertheless, phase flattening occurring close to the high-wavenumber spectral edge (around  $3295$   $\text{cm}^{-1}/3034$  nm) may also contribute to the presence of weak pulsed features and suggest the existence of non-negligible amplitude modulation of the  $E$ -field waveform.

The free-running dual-comb spectrum measured within 1 ms shows beat notes with signal-to-noise ratios (SNRs) reaching up to 25 dB (Fig. 2f). Values higher by 10 dB were also possible, yet the detector and RF electronics responded in a nonlinear fashion producing intermodulation products. Interestingly, the beat note linewidth evolves across the spectrum. The central part near 1 GHz has  $\sim 0.5$  MHz-wide lines, which triples for lines located at the edges. Assuming uncorrelated operation of the devices, the corresponding optical linewidths lie in the 350–1000 kHz range. To better understand the nature of the line broadening phenomenon, we computationally extracted the instantaneous RF offset  $\Delta f_0(t)$  and repetition rate difference  $\Delta f_{\text{rep}}(t)$ . Not only does it allow to prove that the entire DCS signal can be corrected by ap-

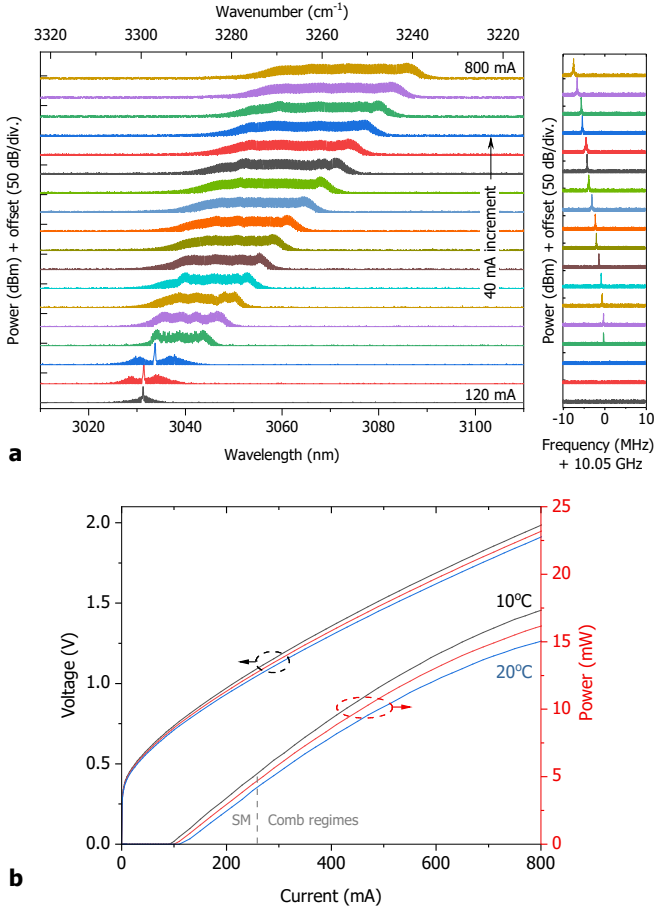


**Figure 3 – Characteristics of the diode lasers.** **a:** Injection current tuning of the optical and microwave spectrum at room temperature. **b:**  $L$ - $I$ - $V$  characteristics of the QWDL devices at different temperatures.

plying global phase correction using the two extracted signals<sup>24</sup>, but also allows us to evaluate the degree of correlation between offset and timing fluctuations. We found that the two are anti-correlated with a correlation coefficient of  $-0.4$ . The symmetric broadening around the comb's center wavelength suggests the existence of a fixed point<sup>25</sup> there, where repetition rate (timing) fluctuations get partially compensated by offset frequency fluctuations. This explanation is in agreement with the recent studies on QCL combs<sup>26</sup>. The obtainable spectral coverage in the DCS experiment reaches  $\sim 520$  GHz, partially limited by the oscilloscope electrical bandwidth, and the lower span of the signal (SIG) comb compared to the local oscillator (LO).

**Tunability** For future application in spectroscopy, it is of practical relevance to characterize the spectral characteristics at different injection currents. This is because semiconductor microcombs often exhibit complex nonlinear dynamics that give rise to highly modulated optical spectra at some biases. Another motivation stems from the attractive perspective of going beyond the coarse GHz mode spacing to perform interleaved gap-less

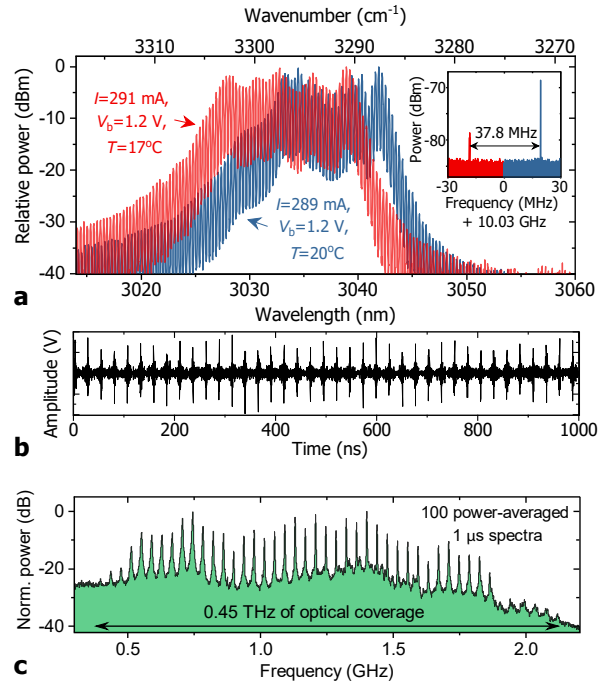


**Figure 4 – Battery-operated mid-infrared dual-comb source.** **a:** Optical spectra of the QWDLs biased at 1.2 V. **b:** Dual-comb beating signal (IFG). **c:** Power-averaged dual-comb spectrum.

spectroscopy<sup>27</sup>.

Unlike in many other comb platforms at MIR wavelengths, the spectral evolution exhibited by the QWDLs (Fig. 3) is monotonic with remarkably smooth spectra, particularly at high higher ( $> 5J_{th}$ ) injection currents. In contrast to QWDLs operating at much shorter wavelengths ( $2 \mu\text{m}$ )<sup>17</sup>, the MIR laser easily switches from single-mode to multi-mode (comb) operation at currents below  $3J_{th}$  ( $\sim 240$  mA). This can be attributed to the longer emission wavelength, which facilitates spatial hole burning (SHB) governing the multi-longitudinal-mode emission mechanism. The so-called carrier grating formed inside the cavity periodically depletes the gain due to standing wave effects, with the period directly proportional to the modal wavelength. However, when the period is too long while carrier diffusion is too slow (i.e. at high injection currents when stimulated emission decreases the carrier lifetime), the laser cannot sustain single-mode lasing. Intuitively, at longer wavelengths this effect will trigger multi-mode lasing more easily. Another important advantage of the MIR QWDL's spectral characteristics is the lack of spectral gaps or multi-lobed envelopes that often arise due to severe modal leakage into the substrate<sup>28</sup>.

The center wavelength of the spectrum tunes in an almost linear fashion by  $\sim 30$  nm ( $32 \text{ cm}^{-1}$ ) over the entire dynamic range of comb operation ( $I=240\text{--}800$  mA). The repetition rate (intermode) beat note does not exhibit any rapid jumps (Fig. 3a, right) and also shows smooth tun-

ing capabilities. In the comb operation range, it shifts by  $\sim 8$  MHz from the nominal value at highest injection currents. The most stable free-running combs are developed at currents ranging from 240 to 400 mA with intermode beat note linewidths below 10 kHz. Higher biases with broader linewidths, however, necessitate microwave injection locking<sup>29</sup> to suppress the timing jitter, as in Fig. 1. A full free-spectral-range (FSR) scan for spectral interleaving requires a change of injection current by  $\sim 45$  mA, which corresponds to an approximate optical tuning coefficient of  $\Delta\nu/\Delta I = 223$  MHz/mA.

**Battery operation** From a power management perspective, the diode topology is highly beneficial<sup>30,31</sup>. The low compliance voltage below 2 V accompanied by moderate injection currents ( $< 1$  A) correspond to near-W electrical power consumption at room temperature when a dozen of mW of optical power per facet are produced. Highly appealing is that in the lowest-noise comb regime (240–400 mA), the compliance voltage is natively compatible with consumer-grade rechargeable NiMH batteries ( $\sim 1.2$  V). This feature encouraged us to implement a battery-operated mid-infrared free-running dual-comb spectrometer. Note that even under such biasing conditions, the amount of emitted optical power ( $> 5$  mW per comb per facet) perfectly fits real-life spectroscopic sensing requirements even with optical path enhancement techniques.

In the proof-of-principle experiment, each QWDL was biased directly from an AA battery without any control circuitry. Except for slightly lowering the spectral overlap and optical bandwidths due to the lower injection currents, other comb parameters remained virtually the same (Fig. 4a) as in the current-stabilized experiment. The temporal structure of the dual-comb IFG preserves its regular spiking. To lower the computational power requirements for a potential instrument, we did not perform any phase correction here prior to obtaining the frequency spectrum. Instead, the Welch periodogram averaging technique<sup>32</sup> was used. It relies on (incoherent) averaging of short-time power spectra to lower the uncertainty of the spectral amplitudes, yet without suppressing the noise floor. Such-processed spectrum (100 averages of 1  $\mu$ s-long signals) plotted in Fig. 4c has a peak SNR of 20 dB, and a total optical coverage of 0.45 THz, which is highly attractive for embedded small-footprint DCS.

**Gain and dispersion** Another important aspect of the MIR QWDLs combs is their group velocity dispersion (GVD), as it governs the ability to phase-lock the longitudinal modes via four-wave mixing (FWM)<sup>22</sup>. We used the Fourier transform technique<sup>33</sup> to study the gain and dispersion characteristics of the SIG device biased close to threshold ( $0.97J_{th}$ ) emitting light via amplified spontaneous emission (ASE). The measured GVD (Fig. 5a) has a mean value of  $+2280$  fs<sup>2</sup>/mm in the 3.02–3.09  $\mu$ m range, which is comparable to other GaSb-based devices

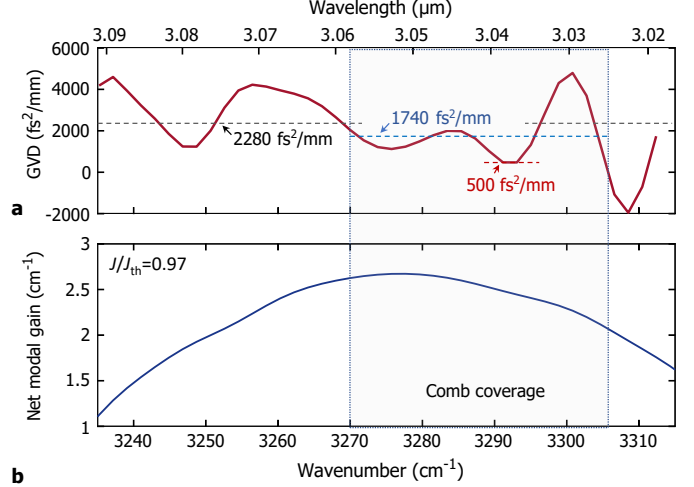


**Figure 5 – Group velocity dispersion (GVD) and gain measurement of the MIR QWDL comb (here SIG laser) at 0.97 of threshold current.** **a:** GVD with the full-range mean of 2280 fs<sup>2</sup>/mm, comb-range mean of 1740 fs<sup>2</sup>/mm, and local minima of as low as 500 fs<sup>2</sup>/mm. **b:** Net modal gain.

like ICLs<sup>18</sup> in the 3  $\mu$ m region, yet still several times higher than long-wave ( $> 7$   $\mu$ m) InP-based QCL devices with negative material dispersion. One of the factors is the highly positive GVD of GaSb<sup>34</sup> ( $> 1000$  fs<sup>2</sup>/mm at 3.05  $\mu$ m), which gets further increased in the device by contributions from the waveguide and gain. Another interesting phenomenon observable in the GVD profile is its oscillatory quasi-periodic shape suggesting minor modal leakage into the high-index GaSb substrate. The period of 25–35 cm<sup>-1</sup> agrees with the prediction based on the substrate thickness ( $150 \pm 20$   $\mu$ m)<sup>28</sup>. While it may be seen as a disadvantage, it allows certain spectral regions to exhibit lower dispersions than nominally without resonant contributions. For instance, in the comb operation range (3270–3305 cm<sup>-1</sup> / 3.025–3.058  $\mu$ m), the mean GVD decreases to 1740 fs<sup>2</sup>/mm with local minima as low as 500 fs<sup>2</sup>/mm. In fact, these low-dispersion regions appearing in the spectrum are not a measurement artifact – they occur exactly where the most stable comb regimes with narrowest linewidths develop (around  $\sim 3292$  cm<sup>-1</sup>). This justifies the need for future dispersion engineering<sup>35</sup> to improve the bandwidth and stability of QWDL combs. The smooth net modal gain (Fig. 5b) clearly supports broadband lasing and does not show any anomalies. Only weak ( $\Delta g < 0.1$  cm<sup>-1</sup>) quasi-periodic sags appear possibly due to resonant (leaky) waveguide losses, yet without causing the laser to lase in multiple lobes.

## Conclusion

In conclusion, we have demonstrated a mid-infrared chip-scale frequency comb platform exploiting the type-I quantum well interband laser medium. The free-running stability exhibited by the lasers allows us to perform

mode-resolved sub-THz-wide DCS around  $3.04\ \mu\text{m}$ . The devices develop single-lobed smooth spectra with excellent tunability and show the potential for future gap-less interleaved spectroscopic measurements of spectrally-narrow molecular absorbers like acetylene ( $\text{C}_2\text{H}_2$ ) or hydrogen cyanide (HCN). Particularly attractive is the low compliance voltage accompanied by low power consumption ( $< 1\ \text{W}$ ), which was used to demonstrate the first battery-operated MIR dual-comb source. When merged with room-temperature interband cascade photodetectors<sup>6,7,8</sup>, the MIR QWDL devices promise dual-comb spectrometers compatible with field-deployable or even space instrument power budgets. The remaining difficulty lies in optimizing the signal processing side, which can potentially benefit from sample rate reduction techniques<sup>36</sup>. Although in this DCS demonstration we used two physical laser chips, two combs on the same chip are also possible. They would constitute a battery-operated MIR dual-comb generator with significant common-mode noise suppression<sup>37</sup> or even an on-chip dual-comb spectrometer<sup>29</sup>. In addition to application in DCS, the QWDL's near-MHz optical linewidths are attractive for other, much simpler mode-resolved cavity-enhanced sensing techniques like Vernier spectroscopy<sup>38</sup>.

## Methods

**3  $\mu\text{m}$  diodes:** The laser wafer was grown at National Research Council (NRC) Canada using solid-source molecular-beam epitaxy (MBE) on a  $n\text{-GaSb}$  (100) substrate. The 2- $\mu\text{m}$ -thick top and bottom cladding layers were formed by Te- and Be-doped  $\text{Al}_{0.6}\text{Ga}_{0.4}\text{As}_{0.052}\text{Sb}_{0.948}$  layers. The laser active region consists of three 10.45-nm-thick  $\text{In}_{0.55}\text{Ga}_{0.45}\text{As}_{0.21}\text{Sb}_{0.79}$  QWs separated by 30-nm-thick  $\text{Al}_{0.2}\text{In}_{0.2}\text{Ga}_{0.6}\text{As}_{0.19}\text{Sb}_{0.81}$  quinary barriers. Heavily-doped GaSb layers are used for the contacts. 3  $\mu\text{m}$  wide ridges were defined photolithographically to ensure single spatial mode emission. The processed wafer was lapped down to a thickness of 150  $\mu\text{m}$ . No coating was deposited onto the facets – they were left as cleaved.

**SWIFTS:** The light emitted by the QWDL was collected using a black-diamond high-numerical-aperture anti-reflective (AR) coated lens, and next guided into a Bruker Vertex 80 FTIR spectrometer with an external photodetector. To prevent dynamic optical feedback that perturbed comb operation during an FTIR scan, an optical isolator was used. The comb device with a natural repetition rate  $f_{\text{rep}} = 10.05\ \text{GHz}$  was weakly (+6 dBm) injection locked using an external microwave generator, which additionally served a phase reference for a fast lock-in amplifier (Zurich Instruments UHFLI). The 10.05 GHz signal, however, was not used directly due to bandwidth limitations of the lock-in. An additional microwave signal offset by 20 MHz was synthesized to drive two mixers: one for the phase reference, and one for down-converting the detected optical signal. Together with the microwave signals, we recorded a DC (normal) IFG to compare the spectrum retrieved from microwave IFGs with the optical one.

**Dual-comb beating:** A pair of QWDL devices cleaved from the same wafer but different bars was slightly detuned in temperature by using thermoelectric coolers ( $\Delta T = 3\ \text{K}$ ) to increase the repetition rate difference  $\Delta f_{\text{rep}}$  and maximize spectral overlap. In the first experiment, the injection currents and temperatures were controlled by a pair of D2-105 drivers (Vescent Photonics). In the battery-operated demonstration, however, no injection current control was

used at all – the diodes were supplied directly from the AA battery's terminals. The optical beams from the two combs were first guided through optical isolators, next attenuated using irises, and finally focused onto a fast thermoelectrically-cooled photodetector (PVI-4TE-3.4, VIGO) equipped with a 2.2 GHz-bandwidth transimpedance preamplifier. Excellent match between the detector responsivity characteristics and the source wavelength ensured high signal-to-noise ratio (SNR) of the electrical beating signal captured by a Lecroy WavePro7Zi-A oscilloscope configured in oversampling 11-bit resolution mode. Because of its limited 1.5 GHz electrical bandwidth, the microwave dual-comb spectra possess a rapid roll-off above 1500 MHz.

**GVD measurement:** The device labeled as SIG was biased below threshold at  $30^\circ\text{C}$ . The collimated ASE light was guided into the step-scan Fourier Transform spectrometer in the same configuration as in the SWIFTS experiment. A low-bandwidth lock-in amplifier (SRS830, Stanford Instruments) was used to measure the interferometrically-modulated light (100 ms time constant). The GVD was retrieved from the second derivative of the roundtrip IFG burst phase spectrum. It should be noted that while the modal leakage effect shows high reproducibility in modulation period (due to the same substrate thickness and modal indices), it displays lower in the location of peaks and troughs. Therefore, devices from the same wafer may possess low-GVD region slightly detuned from one another.

## References

1. Davis, S. P., Abrams, M. C. & Brault, J. W. *Fourier transform spectrometry* (Elsevier, 2001).
2. Hänsch, T. W. Nobel lecture: passion for precision. *Reviews of Modern Physics* **78**, 1297 (2006).
3. Coddington, I., Newbury, N. & Swann, W. Dual-comb spectroscopy. *Optica* **3**, 414 (2016).
4. Stern, B., Ji, X., Okawachi, Y., Gaeta, A. L. & Lipson, M. Battery-operated integrated frequency comb generator. *Nature* **562**, 401–405 (2018).
5. Scalari, G., Faist, J. & Picqué, N. On-chip mid-infrared and THz frequency combs for spectroscopy. *Applied Physics Letters* **114**, 150401 (2019).
6. Lotfi, H. *et al.* Monolithically integrated mid-IR interband cascade laser and photodetector operating at room temperature. *Applied Physics Letters* **109**, 151111 (2016).
7. Schwarz, B. *et al.* Monolithic frequency comb platform based on interband cascade lasers and detectors. *Optica* **6**, 890–895 (2019).
8. Sterczewski, L. A. *et al.* Mid-infrared dual-comb spectroscopy with room-temperature bi-functional interband cascade lasers and detectors. *Applied Physics Letters* **116**, 141102 (2020).
9. Hugi, A., Villares, G., Blaser, S., Liu, H. C. & Faist, J. Mid-infrared frequency comb based on a quantum cascade laser. *Nature* **492**, 229–233 (2012).
10. Bagheri, M. *et al.* Passively mode-locked interband cascade optical frequency combs. *Scientific Reports* **8**, 3322 (2018).
11. Sterczewski, L. A. *et al.* Multiheterodyne spectroscopy using interband cascade lasers. *Optical Engineering* **75**, 011014 (2017).
12. Feng, T., Shterengas, L., Hosoda, T., Belyanin, A. & Kipshidze, G. Passive Mode-Locking of 3.25  $\mu\text{m}$  GaSb-Based Cascade Diode Lasers. *ACS Photonics* **5**, 4978–4985 (2018).
13. Lu, Q. Y., Manna, S., Wu, D. H., Slivken, S. & Razeghi, M. Shortwave quantum cascade laser frequency comb for multiheterodyne spectroscopy. *Applied Physics Letters* **112**, 141104 (2018).
14. Kazakov, D. *et al.* Self-starting harmonic frequency comb generation in a quantum cascade laser. *Nature Photonics* **11**, 789–792 (2017).
15. Sterczewski, L. A. *et al.* Mid-infrared dual-comb spectroscopy

- with interband cascade lasers. *Optics Letters* **44**, 2113–2116 (2019).
16. Feng, T. *et al.* Passively mode-locked 2.7 and 3.2  $\mu\text{m}$  GaSb-Based cascade diode lasers. *Journal of Lightwave Technology* **38**, 1895–1899 (2020).
  17. Sterczewski, L. A., Frez, C., Forouhar, S., Burghoff, D. & Bagheri, M. Frequency-modulated diode laser frequency combs at 2  $\mu\text{m}$  wavelength. *APL Photonics* **5**, 076111 (2020).
  18. Sterczewski, L. *et al.* Waveguiding and dispersion properties of interband cascade laser frequency combs. In *Novel In-Plane Semiconductor Lasers XX*, vol. 11705, 1170519 (International Society for Optics and Photonics, 2021).
  19. Piccardo, M. *et al.* The harmonic state of quantum cascade lasers: Origin, control, and prospective applications [Invited]. *Optics Express* **26**, 9464 (2018).
  20. Sterczewski, L. A. *et al.* Interband cascade laser frequency combs. *Journal of Physics: Photonics* **3**, 042003 (2021).
  21. Burghoff, D. *et al.* Evaluating the coherence and time-domain profile of quantum cascade laser frequency combs. *Optics Express* **23**, 1190 (2015).
  22. Opačak, N. & Schwarz, B. Theory of frequency modulated combs in lasers with spatial hole burning, dispersion and Kerr. *Physical Review Letters* **123**, 243902 (2019).
  23. Burghoff, D. Unraveling the origin of frequency modulated combs using active cavity mean-field theory. *Optica* **7**, 1781 (2020).
  24. Sterczewski, L. A., Westberg, J. & Wysocki, G. Computational coherent averaging for free-running dual-comb spectroscopy. *Optics Express* **27**, 23875–23893 (2019).
  25. Walker, D., Udem, T., Gohle, C., Stein, B. & Hänsch, T. Frequency dependence of the fixed point in a fluctuating frequency comb. *Applied Physics B* **89**, 535–538 (2007).
  26. Shehzad, A. *et al.* Frequency noise correlation between the offset frequency and the mode spacing in a mid-infrared quantum cascade laser frequency comb. *Optics Express* **28**, 8200 (2020).
  27. Gianella, M. *et al.* High-resolution and gapless dual comb spectroscopy with current-tuned quantum cascade lasers. *Optics Express* **28**, 6197–6208 (2020).
  28. Bewley, W. *et al.* Antimonide type-II “W” lasers: growth studies and guided-mode leakage into substrate. *Physica E: Low-dimensional Systems and Nanostructures* **20**, 466–470 (2004).
  29. Hillbrand, J., Andrews, A. M., Detz, H., Strasser, G. & Schwarz, B. Coherent injection locking of quantum cascade laser frequency combs. *Nature Photonics* **13**, 101–104 (2019).
  30. Day, M. W. *et al.* Simple single-section diode frequency combs. *APL Photonics* **5**, 121303 (2020).
  31. Dong, M., Day, M. W., Winful, H. G. & Cundiff, S. T. Quantum-well laser diodes for frequency comb spectroscopy. *Optics Express* **28**, 21825–21834 (2020).
  32. Welch, P. The use of fast Fourier transform for the estimation of power spectra: a method based on time averaging over short, modified periodograms. *IEEE Transactions on Audio and Electroacoustics* **15**, 70–73 (1967).
  33. Hofstetter, D. & Faist, J. Measurement of semiconductor laser gain and dispersion curves utilizing fourier transforms of the emission spectra. *IEEE Photonics Technology Letters* **11**, 1372–1374 (1999).
  34. Adachi, S. Optical dispersion relations for GaP, GaAs, GaSb, InP, InAs, InSb,  $\text{Al}_x\text{Ga}_{1-x}\text{As}$ , and  $\text{In}_{1-x}\text{Ga}_x\text{As}_y\text{P}_{1-y}$ . *Journal of Applied Physics* **66**, 6030–6040 (1989).
  35. Villares, G. *et al.* Dispersion engineering of quantum cascade laser frequency combs. *Optica* **3**, 252–258 (2016).
  36. Sterczewski, L. A. & Bagheri, M. Subsampling dual-comb spectroscopy. *Optics Letters* **45**, 4895–4898 (2020).
  37. Westberg, J., Sterczewski, L. & Wysocki, G. Mid-infrared multi-heterodyne spectroscopy with phase-locked quantum cascade lasers. *Applied Physics Letters* **110**, 141108 (2017).
  38. Sterczewski, L. A. *et al.* Cavity-enhanced vernier spectroscopy with a chip-scale mid-infrared frequency comb. *Submitted* (2021).

### Acknowledgements

This work was supported under National Aeronautics and Space Agency’s (NASA) PICASSO program (106822 / 811073.02.24.01.85), and Research and Technology Development Spontaneous Concept Fund. It was in part performed at the Jet Propulsion Laboratory (JPL), California Institute of Technology, under contract with the NASA. L. A. Sterczewski’s research was supported by an appointment to the NASA Postdoctoral Program at JPL, administered by Universities Space Research Association under contract with NASA.

### Author contributions

L.A.S., M.F., and M.B. conceived the idea. L.A.S. carried out the optical and electrical measurements, and analyzed the data. S.F. designed the laser structures. C.F. fabricated the devices reported here. L.A.S and M.B. wrote the manuscript with input from all authors. M.B. coordinated the project.

### Conflict of interest

The authors declare no conflict of interest.

### Data availability statement

The data that support the plots within this paper and other findings of this study are available from the corresponding author upon reasonable request.